Association of Near-Infrared and Short-Wavelength Autofluorescence With the Retinal Sensitivity in Eyes With Resolved Central Serous Chorioretinopathy

Hirotsugu Soga,[1] Ryo Asaoka,[1,3,4] Kazuaki Kadonosono,[2] Maiko Maruyama-Inoue,[2] Nozomi Igarashi,[1] Marie Kitano,[1] Kohdai Kitamoto,[1] Keiko Azuma,[1] Ryo Obata,[1] and Tatsuya Inoue[1,2]

[1]Department of Ophthalmology, Graduate School of Medicine and Faculty of Medicine, The University of Tokyo, Bunkyo-ku, Tokyo, Japan
[2]Department of Ophthalmology and Micro-Technology, Yokohama City University School of Medicine, Minami-ku, Yokohama, Kanagawa, Japan
[3]Department of Ophthalmology, Seirei Hamamatsu General Hospital, Shizuoka, Japan
[4]Seirei Christopher University, Shizuoka, Japan

Correspondence: Tatsuya Inoue, Department of Ophthalmology and Micro-Technology, Yokohama City University School of Medicine, 4-57 Urafune, Minami-ku, Yokohama 232-0024, Japan; inouet-tky@umin.ac.jp.

Received: November 28, 2020
Accepted: March 4, 2021
Published: March 25, 2021

Citation: Soga H, Asaoka R, Kadonosono K, et al. Association of near-infrared and short-wavelength autofluorescence with the retinal sensitivity in eyes with resolved central serous chorioretinopathy. *Invest Ophthalmol Vis Sci.* 2021;62(3):36. https://doi.org/10.1167/iovs.62.3.36

Purpose. The purpose of this study was to compare the results of near-infrared autofluorescence (NIRAF) and short-wavelength autofluorescence (SWAF) imaging of eyes with resolved central serous chorioretinopathy (CSC) and to assess the retinal sensitivity (RS) in areas with abnormal autofluorescence (AF) using white-on-white (WW) and blue-on-yellow (BY) perimetries.

Methods. We examined 20 consecutive eyes with resolved CSC. We calculated the areas of abnormal AF detected by SWAF and NIRAF imaging as SWAF_area and NIRAF_area, respectively, and the number of measurement points within and outside abnormal SWAF and NIRAF regions were counted. The results of WW and BY perimetries were superimposed on the AF images, and the mean overall RS within and outside abnormal SWAF and NIRAF regions were calculated using both WW and BY perimetries (W-RSin_SWAF, W-RSout_SWAF, W-RSin_NIRAF, W-RSout_NIRAF, B-RSin_SWAF, B-RSout_SWAF, B-RSin_NIRAF, and B-RSout_NIRAF, respectively).

Results. The mean age of the participants was 54.1 years. The SWAF_area was significantly smaller than the NIRAF_area ($P < 0.0001$, Wilcoxon signed rank test). A χ^2 test suggested a significant relationship between the number of measurement points within/outside abnormal SWAF and NIRAF regions ($P < 0.0001$). In the results of measurement by WW perimetry, there was a significant difference between W-RSin_NIRAF and W-RSout_NIRAF ($P < 0.0001$), but not between W-RSin_SWAF and W-RSout_SWAF ($P = 0.060$, Wilcoxon rank sum test). In contrast, on BY perimetry, there were significant differences between both B-RSin_SWAF and B-RSout_SWAF and between B-RSin_NIRAF and B-RSout_NIRAF ($P < 0.0001$).

Conclusions. NIRAF was useful for predicting impaired RS in eyes with resolved CSC.

Keywords: central serous chorioretinopathy (CSC), near-infrared autofluorescence (NIRAF), blue-on-yellow perimetry

Central serous chorioretinopathy (CSC) is characterized by serous retinal detachment (SRD) of the neurosensory retina accompanied by dysfunction of the retinal pigment epithelium (RPE).[1,2] Visual function often fully recovers spontaneously with the resolution of SRD; however, an impaired visual acuity (VA) or retinal sensitivity (RS) persists in some patients, even after the resolution of SRD.

Fundus autofluorescence (AF) can be measured noninvasively and can provide critical information for the diagnosis of several macular diseases, including CSC.[3–6]Two modalities of AF imaging have been used: short-wavelength AF (SWAF) and near-infrared AF (NIRAF) imaging. For fundus imaging, SWAF is more common than NIRAF. The latter images are best acquired with the Heidelberg Retina Angiograph 2 (HRA2; Heidelberg Engineering). By comparison, with the Spectralis HRA + OCT, which is more often utilized in clinic centers, NIRAF signal intensity is reduced, resulting in less than optimal NIRAF image quality. Few studies have investigated the usefulness of NIRAF imaging in eyes with CSC. Kim et al. reported that abnormal AF areas were more noticeable with NIRAF than with SWAF in eyes with resolved CSC.[7] The SWAF signal (488 nm excitation) is derived from the lipofuscin pigment of RPE cells,[8,9] whereas the NIRAF signal (787 nm excitation) originates

from melanin in the RPE and choroid.[10] Indeed, melanin and its related compounds (melanolipofuscin, melanolysosomes, and oxidized melanin) have been ascertained using NIRAF imaging in eyes with geographic atrophy.[11] Other studies have reported that diagnosis and evaluation of visual functions by NIRAF imaging in eyes with retinitis pigmentosa with an AF ring are comparable to those by SWAF imaging.[12,13] In the current study, we attempted to compare the results of NIRAF and SWAF imaging in eyes with resolved CSC.

In addition to the assessment by white-on-white (WW) perimetry, we assessed the RS in the affected areas using blue-on-yellow (BY) perimetry. BY perimetry, also known as short-wavelength automated perimetry, uses a short-wavelength stimulus on a high-luminance yellow background. BY perimetry can be used to measure the blue cone function separately from that of other cones and has been useful in detecting damage to visual function in various diseases, such as glaucoma[14,15] and diabetic retinopathy,[16,17] earlier than conventional WW perimetry. Furthermore, we recently reported the usefulness of this approach in the region of SRD in eyes with CSC.[18] We, therefore, compared the RS measured using WW and BY perimetries in eyes with resolved CSC, and investigated the relationships between the RS assessed using the two types of perimetry and AF imaging.

Methods

This was a retrospective observational case series study conducted at the University of Tokyo, School of Medicine, Tokyo, Japan, with the approval of the Institutional Review Board of the University of Tokyo Hospital (Approval ID: 3770). Informed consent was obtained from all the patients. All data were anonymized. The study protocol adhered to the tenets of the Declaration of Helsinki.

All patients underwent comprehensive ophthalmological examinations, including measurements of the best-corrected VA and intraocular pressure as well as anterior segment and funduscopic examinations under pupillary dilation. The diagnosis of CSC was made based on optical coherence tomography (OCT), fluorescein angiography, and indocyanine green angiography findings. All patients also underwent BY and WW perimetry on the same day. We excluded patients with (1) a history of ocular surgery (other than uncomplicated cataract surgery); (2) other retinal disorders, including cataract, that can cause visual function deterioration; and (3) choroidal neovascularization and polypoidal choroidal vasculopathy.

Optical Coherence Tomography Measurement

OCT images were obtained using a spectral-domain OCT device (Heidelberg Engineering, Heidelberg, Germany). All OCT images consisted of line scans (horizontal and vertical B-scans) and raster scans (25 horizontal B-scans). The central retinal thickness (CRT) and central choroidal thickness (CCT) were measured in the enhanced depth imaging (EDI) mode. In addition, the area of ellipsoid zone (EZ) disruption was identified and calculated as EZ_area for each eye, as per the protocol followed in our previous study on retinitis pigmentosa.[19]

Fundus Autofluorescence Measurement

AF images were obtained using a confocal laser scanning ophthalmoscope (HRA2; Heidelberg Engineering, Heidelberg, Germany) within 30 degrees at a resolution of 768 × 768 pixels. For the SWAF imaging, a wavelength of 488 nm was used for excitation, and the emitted light was above 500 nm and detected through a barrier filter. For the NIRAF images, a wavelength of 787 nm was used for excitation, and the emitted light was above 810 nm. In all the examined eyes, the areas of abnormal AF were measured in both the SWAF and NIRAF images as SWAF_area and NIRAF_area, respectively.

Retinal Sensitivity Measurement

Both WW and BY perimetric tests were performed using an AP-7000 automatic perimeter (KOWA Company Ltd., Tokyo, Japan), as in our previously reported study.[18] Before the measurement of RS with AP-7000, the fixation point was checked using MP-3 microperimetry (Nidek Co. Ltd., Aichi, Japan) for all patients. The RS thresholds were measured at 68 test points corresponding to the Humphrey Field Analyzer (Carl-Zeiss Meditec, Dublin, CA, USA) 10-2 program. BY perimetry was conducted using a short-wavelength (450 nm) stimulus that was presented for 200 ms and by projection of the target on a yellow background (600 nm with a brightness of 100 cd/m^2). The BY and WW perimetric tests were performed in random order. The results of the BY and WW perimetric tests were registered on the SWAF and NIRAF images using the built-in software in the AP-7000 automatic perimeter (Fig. 1).

The mean overall RS was calculated using WW (W-RS) and BY (B-RS) perimetries. Furthermore, the mean RS within (W-RSin, B-RSin) and outside (W-RSout, B-RSout), the abnormal SWAF and NIRAF regions were calculated (W-RSin_SWAF, W-RSin_NIRAF, B-RSin_SWAF, B-RSin_NIRAF, W-RSout_SWAF, W-RSout_NIRAF, B-RSout_SWAF, and B-RSout_NIRAF, respectively).

Statistical Analysis

The SWAF_area and NIRAF_area were compared using an exact Wilcoxon signed-rank test. To investigate the relationship between the SWAF and NIRAF measurements, we counted the number of measurement points inside and outside abnormal SWAF and NIRAF regions, and the relationship between the number of points within/outside abnormal SWAF and NIRAF regions was analyzed using a χ^2 test. Comparisons were also conducted (1) between W-RSin_SWAF and W-RSout_SWAF, (2) W-RSin_NIRAF and W-RSout_NIRAF, (3) B-RSin_SWAF with B-RSout_SWAF, and (4) B-RSin_NIRAF with B-RSout_NIRAF, using a Wilcoxon rank sum test.

To investigate the relationship between the duration of time after the resolution of SRD and each of the baseline parameters, a multivariate linear regression analysis was conducted. We counted the number of measurement points inside and outside EZ disruption areas, and the relationships (1) between points within/outside abnormal SWAF region and within/outside EZ disruption areas, and (2) between points within/outside abnormal NIRAF region and within/outside EZ disruption areas were analyzed using a χ^2 test. We further analyzed the relationship between the RS measured using WW or BY perimetry

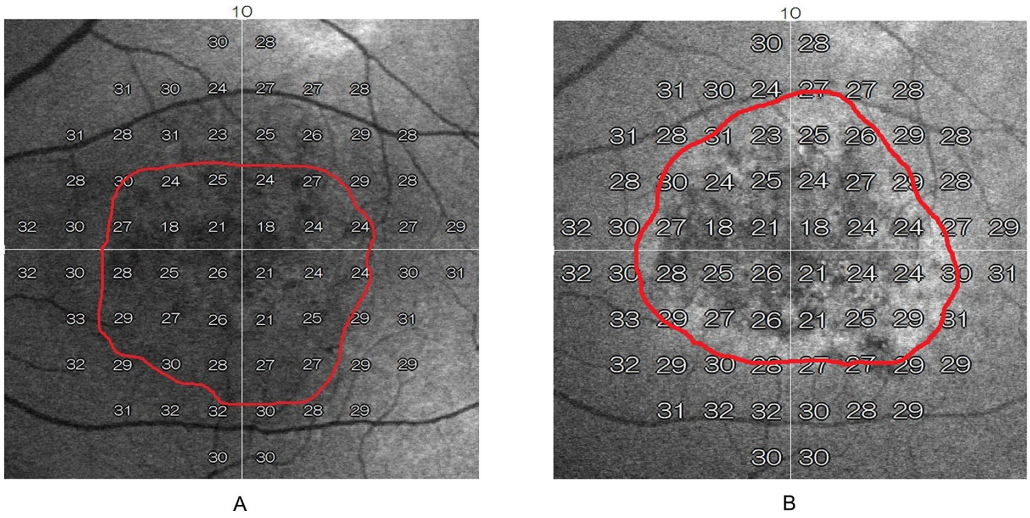

Figure 1. Representative areas of abnormal signals on NIRAF (**A**) and SWAF (**B**) imaging superimposed by the perimetry results using the built-in software in the AP-7000 perimeter. The damaged area is inside the *red curved line*. NIRAF, near-infrared autofluorescence; SWAF, short-wavelength autofluorescence.

at all measurement points and age, SWAF classification (within/outside abnormal SWAF region), NIRAF classification (within/outside abnormal NIRAF region), and EZ classification (within/outside EZ disruption area) were analyzed using a linear mixed model.

All statistical analyses were performed using the statistical programming language "R" (R version 3.5.1; The R Foundation for Statistical Computing, Vienna, Austria).

Results

The baseline characteristics of the 20 patients with resolved CSC enrolled in the present study are shown in Table 1. The mean age of the patients was 54.1 ± 10.0 (mean ± standard deviation) years and the mean logMAR best-corrected VA (logMAR VA) was 0.000066 ± 0.14. The CRT and CCT were 201.8 ± 36.8 µm and 369.2 ± 107.4 µm, respectively. The duration of time after SRD resolution was 15.2 ± 12.1 months. EZ_area was 3.07 ± 4.6 mm^2, and no disruption area was observed in 9 eyes with resolved CSC. W-RS and B-RS were 30.7 ± 2.3 dB and 26.6 ± 3.9 dB, respectively, and the difference between W-RS and B-RS was statistically significant ($P < 0.0001$, Wilcoxon signed rank test).

SWAF_area (3.11 ± 5.0 mm^2) was significantly smaller than NIRAF_area (5.64 ± 5.9 mm^2, $P < 0.0001$, Wilcoxon signed rank test). Among all the 1360 (68 × 20) measurement points, the number of measurement points within and outside abnormal SWAF region were 200 and 1160, respectively, and those within and outside abnormal NIRAF region were 363 and 997, respectively. We found a significant relationship between the number of points within/outside abnormal SWAF and NIRAF regions ($P < 0.0001$, Table 2).

There was a significant difference between W-RSin_NIRAF and W-RSout_NIRAF ($P < 0.0001$), whereas no significant difference was observed between W-RSin_SWAF and W-RSout_SWAF ($P = 0.060$, Wilcoxon rank sum test; Figs. 2A, 2B). In contrast, the measurement by BY perimetry revealed significant differences between (i) B-RSin_SWAF and B-RSout_SWAF and (ii) B-RSin_NIRAF and B-RSout_NIRAF ($P < 0.0001$, respectively, Wilcoxon rank sum test, Figs. 3A, 3B).

Table 1. Subject Demographics

	Mean ± SD	Range
Eyes	20	–
Gender, M : F	13 : 7	–
Age, y	54.1 ± 10.0	41 – 77
LogMAR VA	0.000066 ± 0.14	−0.18 to 0.40
CRT, µm	201.8 ± 36.8	106.0 – 255.0
CCT, µm	369.2 ± 107.4	186.0 – 609.0
SWAF_area, mm^2	3.11 ± 5.0	0 – 21.6
NIRAF_area, mm^2	5.64 ± 5.9	0.24 – 21.7
EZ_area, mm^2	3.07 ± 4.6	0 – 17.6
W-RS, dB	30.7 ± 2.3	16 – 37
W-RSin_SWAF, dB	30.4 ± 2.4	18 – 36
W-RSout_SWAF, dB	30.8 ± 2.3	16 – 37
W-RSin_NIRAF, dB	30.3 ± 2.4	19 – 37
W-RSout_NIRAF, dB	30.8 ± 2.2	16 – 37
B-RS, dB	26.6 ± 3.9	2 – 38
B-RSin_SWAF, dB	24.2 ± 3.8	2 – 33
B-RSout_SWAF, dB	27.0 ± 3.7	15 – 38
B-RSin_NIRAF, dB	25.0 ± 4.0	2 – 36
B-RSout_NIRAF, dB	27.2 ± 3.7	9 – 38

SD, standard deviation; logMAR, logarithm of the minimum angle of resolution; VA, visual acuity; W-RS, mean overall retinal sensitivity (RS) assessed by white-on-white perimetry; W-RSin, mean RS inside the abnormal autofluorescence region assessed by WW perimetry; W-RSout, mean RS outside the abnormal autofluorescence region assessed by WW perimetry; B-RS, mean overall RS assessed by blue-on-yellow perimetry; B-RSin, mean RS inside the abnormal autofluorescence region assessed by blue-on-yellow perimetry; B-RSout, mean RS outside the abnormal autofluorescence region assessed by blue-on-yellow perimetry; SWAF_area, mean abnormal autofluorescence area on short-wavelength autofluorescence imaging; NIRAF_area, mean abnormal autofluorescence area on near-infrared autofluorescence imaging; CRT, central retinal thickness; CCT, central choroidal thickness.

Multivariate linear regression analysis suggested that the duration of time after the resolution of SRD was not related to most of the baseline parameters (age, logMAR VA, W-RS, B-RS, CRT, CCT, SWAF_area, NIRAF_area, and the difference between W-RSin_SWAF and W-RSout_SWAF,

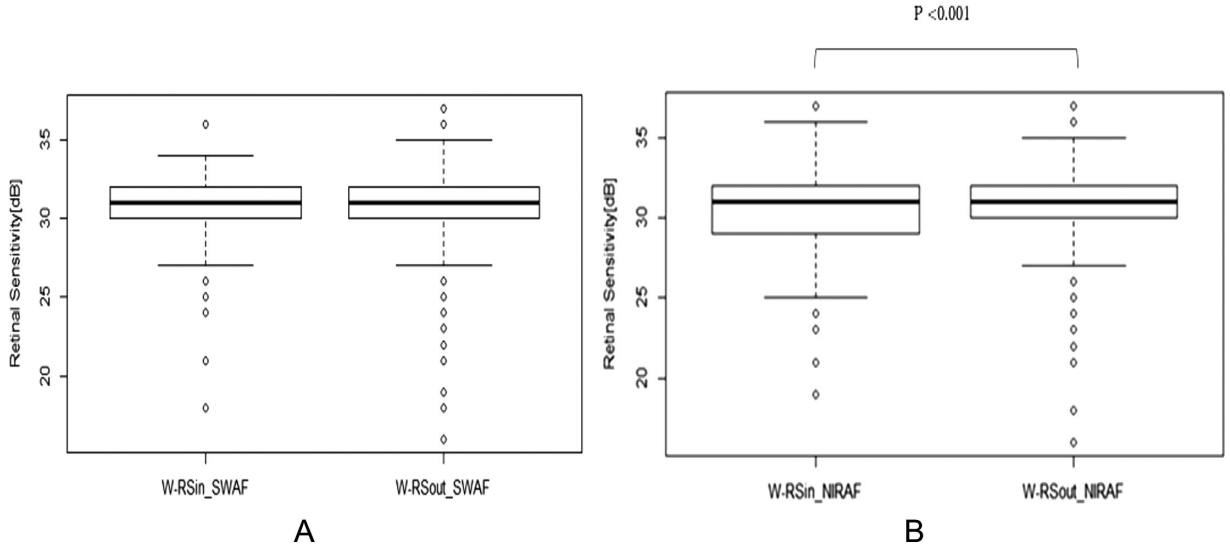

Figure 2. RS within and outside the area of abnormal autofluorescence in SWAF (**A**) and NIRAF (**B**) images measured by WW perimetry. **A** There was no significant difference between W-RSin_SWAF and W-RSout_SWAF ($P = 0.060$, Wilcoxon rank sum test). **B** There was a significant difference between W-RSin_NIRAF and W-RSout_NIRAF ($P < 0.0001$, Wilcoxon rank sum test). W-RSin_SWAF, RS within the area of abnormal autofluorescence in SWAF images measured by WW perimetry; W-RSout_SWAF, RS outside the area of abnormal autofluorescence in SWAF images measured by WW perimetry; W-RSin_NIRAF, RS within the area of abnormal autofluorescence in NIRAF images measured by WW perimetry; W-RSout_NIRAF, RS outside the area of abnormal autofluorescence in NIRAF images measured by WW perimetry.

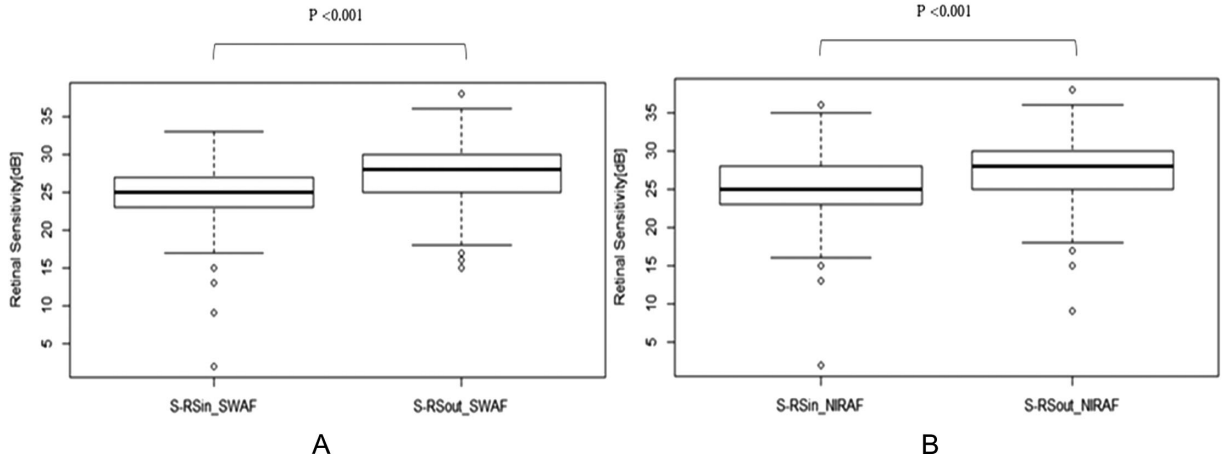

Figure 3. RS within and outside the area of abnormal autofluorescence region in SWAF (**A**) and NIRAF (**B**) images measured by BY perimetry. **A** There was a significant difference between B-RSin_SWAF and B-RSout_SWAF ($P < 0.001$, Wilcoxon rank sum test). **B** There was a significant difference between B-RSin_NIRAF and B-RSout_NIRAF ($P < 0.0001$, Wilcoxon rank sum test). B-RSin_SWAF, RS within the area of abnormal autofluorescence in SWAF images measured by blue-on-yellow perimetry; B-RSout_SWAF, RS outside the area of abnormal autofluorescence in SWAF images measured by blue-on-yellow perimetry; B-RSin_NIRAF, RS within the area of abnormal autofluorescence in NIRAF images measured by blue-on-yellow perimetry; B-RSout_NIRAF, RS outside the area of abnormal autofluorescence in NIRAF images measured by blue-on-yellow perimetry.

$P > 0.05$, respectively), but with the difference between W-RSin_NIRAF and W-RSout_NIRAF ($P = 0.0037$, linear regression analysis).

The number of measurement points within and outside EZ disruption area was 129 and 1231, respectively. The χ^2 test revealed significant associations between EZ disruption area and abnormal SWAF region and between EZ disruption area and abnormal NIRAF region ($P < 0.0001$, respectively).

Among the age, SWAF classification (within/outside abnormal SWAF region), NIRAF classification (within/outside abnormal NIRAF region), EZ classification (within/outside EZ disruption area), age and EZ classification were significantly associated with the RS measured using WW perimetry ($P = 0.0025$ and $P < 0.0001$, respectively, linear mixed model). On the other hand, all four variables were significantly correlated with the RS

Table 2. The Number of Points Inside and Outside the Abnormal Regions in SWAF and NIRAF

	Inside NIRAF	Outside NIRAF	Total
Inside SWAF	162	38	200
Outside SWAF	201	959	1160
Total	363	997	1360

There was a significant relationship between the number of points within/outside the abnormal SWAF and NIRAF regions ($P < 0.0001$, χ^2 test).

SWAF, short-wavelength autofluorescence imaging; NIRAF, near-infrared autofluorescence imaging.

measured using BY perimetry ($P = 0.034$, $P < 0.0001$, $P = 0.0016$, and $P < 0.0001$, respectively, linear mixed model).

Discussion

In the present study, we compared the results of NIRAF imaging with SWAF imaging for eyes with resolved CSC. The RS within and outside the abnormal AF areas was calculated, and the results revealed a significant difference in the RS measured by WW perimetry within and outside the abnormal NIRAF region, but no such difference was seen between those within and outside the abnormal SWAF region. However, there were significant differences in the RS measured by BY perimetry within and outside the abnormal SWAF and NIRAF regions.

AF measurements have become a routine method for evaluating retinal disease progression because they provide information on alterations in the RPE cells. Previous studies have suggested different levels of usefulness for SWAF and NIRAF imaging in evaluating various retinal diseases. In retinitis pigmentosa, both SWAF and NIRAF imaging have been useful to monitor disease progression.[12] Moreover, in cases of retinitis pigmentosa, where an AF ring is observed in the macula, Jauregui et al. quantitatively compared the usefulness of the two AF modalities in monitoring disease progression.[13] Both imaging modalities revealed similar rates of disease progression; however, NIRAF imaging is preferred as the primary tool for tracking disease progression over the more commonly used SWAF imaging because it is associated with increased patient comfort and cooperation during imaging. In Stargardt disease, the hypoAF area on NIRAF imaging exceeded the region of EZ band loss, and corresponded to the outer-segment thinned area, indicating that NIRAF imaging enables the prediction of the loss of photoreceptors by detecting RPE cell loss.[20] Additionally, in Stargardt disease, Duncker et al. reported that EZ disruption was observed at sites where the NIRAF signal was reduced.[21] They also suggested that the lesion area was delineated better in NIRAF images as compared with SWAF images. The area of low NIRAF exceeded the area of EZ disruption in some patients. A more recent study suggested that detection of lesions with NIRAF imaging was superior to that with SWAF imaging in eyes with CSC when the lesion occupied the central retina. Han et al. indicated that the dark signal of the affected area contrasted with the central brightness in NIRAF images, whereas the macular pigment-associated reduction in the AF signal hampered the detection of CSC lesions on SWAF images.[22] Kim et al. reported that although the abnormal SWAF signals corresponded to the EZ disruption area, abnormal NIRAF signals were not related to EZ disruption in patients with resolved CSC.[7] They also reported that the NIRAF signals correlated with the location of the window defect in fluorescein angiography. Moreover, NIRAF imaging can detect the dysfunction of RPE cells even before the impairment of the photoreceptor cells occurs in eyes with CSC. Our current study indicated that the NIRAF_area was significantly larger than the SWAF_area, and, as a result, significantly more test points were located within the abnormal NIRAF region than within the abnormal SWAF region, which may suggest that changes in NIRAF imaging precede those on SWAF imaging. Consistent with a previous report by Kim et al., our present results suggested that SWAF was significantly related to EZ disruption, whereas NIRAF was also associated with EZ disruption. However, in the present study, the EZ_area was relatively small in all examined eyes (9 eyes had no EZ disruption); therefore, future studies are needed to precisely clarify the correlation between EZ disruption and AF signal in eyes with CSC. To further verify that changes in NIRAF imaging precede those in SWAF imaging, we conducted VF measurements using WW and BY perimetries.

Recently, we reported that the RS measured with BY perimetry more precisely reflects the presence of subretinal fluid than that measured by WW perimetry in CSC eyes with SRD.[18] Point-wise analysis in the current study suggested that the RS, as measured by WW perimetry, was reduced within the abnormal NIRAF region as compared with that outside the abnormal NIRAF region, whereas there was no significant difference in the RS within and outside the abnormal SWAF region. In contrast, a significant reduction in RS was observed within both the abnormal SWAF and NIRAF regions when BY perimetry was used. These findings may suggest that both changes in the abnormal NIRAF and SWAF regions may be associated with deterioration of the RS (as suggested by the results with BY perimetry); however, it may be more sensitively reflected by changes in abnormal NIRAF region than by those in abnormal SWAF region (as suggested by the results of WW perimetry). In addition, we found that the duration of time after the resolution of SRD significantly correlated with the difference between W-RSin_NIRAF and W-RSout_NIRAF. This result suggested that NIRAF imaging was not only useful for predicting RS but also for predicting the duration after the resolution of the fluid in eyes with CSC.

This study had some limitations. First, this study was retrospective and cross-sectional in nature; therefore, we could not evaluate the changes in the AF areas over time. Ayata et al. reported that granular AF, corresponding to the previously detached area, appears earlier in SWAF images, but disappears later in the NIRAF images after CSC resolution.[23] Another work suggested that the increased SWAF signals in CSC appear to return to baseline values about 4 months after subretinal fluid resolution.[24] Further studies are needed to clarify the relationship between AF images and visual function; moreover, it would be interesting to investigate the temporal changes in fundus AF and RS. Second, TD values could not be obtained from BW perimetry measured with AP-7000. An accurate evaluation could be achieved by considering the eccentricity within the investigated area.

In conclusion, the area of the abnormal signals on NIRAF imaging (abnormal NIRAF region) was significantly larger than that on SWAF imaging (abnormal SWAF region), and the abnormal areas revealed in the two images overlapped in eyes with CSC. The RS measured by WW perimetry was reduced within the abnormal NIRAF region and that

measured by BY perimetry was reduced in both abnormal SWAF and NIRAF regions, suggesting the usefulness of NIRAF imaging for predicting impaired RS in eyes with resolved CSC.

Acknowledgments

Disclosure: **H. Soga**, None; **R. Asaoka**, None; **K. Kadonosono**, None; **M. Maruyama-Inoue**, None; **N. Igarashi**, None; **M. Kitano**, None; **K. Kitamoto**, None; **K. Azuma**, None; **R. Obata**, None; **T. Inoue**, None

References

1. Daruich A, Matet A, Dirani A, et al. Central serous chorioretinopathy: RECENT findings and new physiopathology hypothesis. *Prog Retin Eye Res*. 2015;48:82–118.
2. Liew G, Quin G, Gillies M, Fraser-Bell S. Central serous chorioretinopathy: a review of epidemiology and pathophysiology. *Clin Exp Ophthalmol*. 2013;41(2):201–214.
3. Imamura Y, Fujiwara T, Spaide RF. Fundus autofluorescence and visual acuity in central serous chorioretinopathy. *Ophthalmology*. 2011;118:700–705.
4. Han J, Cho NS, Kim K, et al. Fundus autofluorescence patterns in central serous chorioretinopathy. *Retina (Philadelphia, Pa)*. 2020;40:1387–1394.
5. Ly A, Nivison-Smith L, Assaad N, Kalloniatis M. *Fundus Autofluorescence in Age-related Macular Degeneration*. Philadelphia, PA: Lippincott Williams and Wilkins; 2017:246–259.
6. Oishi A, Oishi M, Ogino K, Morooka S, Yoshimura N. *Wide-field fundus autofluorescence for retinitis pigmentosa and cone/cone-rod dystrophy*. New York LLC: Springer; 2016:307–313.
7. Kim SK, Kim SW, Oh J, Huh K. Near-infrared and short-wavelength autofluorescence in resolved central serous chorioretinopathy: association with outer retinal layer abnormalities. *Am J Ophthalmol*. 2013;156(1):157–164.e2.
8. Delori FC, Dorey CK, Staurenghi G, Arend O, Goger DG, Weiter JJ. In vivo fluorescence of the ocular fundus exhibits retinal pigment epithelium lipofuscin characteristics. *Invest OphthalmolVis Sci*. 1995;36:718–729.
9. Sparrow JR, Wu Y, Kim CY, Zhou J. Phospholipid meets all-trans-retinal: the making of RPE bisretinoids. *J Lipid Res*. 2010;51(2):247–261.
10. Keilhauer CN, Delori FC. Near-infrared autofluorescence imaging of the fundus: visualization of ocular melanin. *Invest Ophthalmol Vis Sci*. 2006;47:3556–3564.
11. Bonilha VL, Bell BA, Hu J, et al. Geographic atrophy: confocal scanning laser ophthalmoscopy, histology, and inflammation in the region of expanding lesions. *Invest OphthalmolVis Sci*. 2020;61:15–15.
12. Duncker T, Tabacaru MR, Lee W, Tsang SH, Sparrow JR, Greenstein VC. Comparison of near-infrared and short-wavelength autofluorescence in retinitis pigmentosa. *Invest Ophthalmol Vis Sci*. 2013;54:585–591.
13. Jauregui R, Park KS, Duong JK, Sparrow JR, Tsang SH. Quantitative comparison of near-infrared versus short-wave autofluorescence imaging in monitoring progression of retinitis pigmentosa. *Am J Ophthalmol*. 2018;194:120–125.
14. van der Schoot J, Reus NJ, Colen TP, Lemij HG. The ability of short-wavelength automated perimetry to predict conversion to glaucoma. *Ophthalmology*. 2010;117:30–34.
15. Bengtsson B, Heijl A. Diagnostic sensitivity of fast blue-yellow and standard automated perimetry in early glaucoma. A comparison between different test programs. *Ophthalmology*. 2006;113:1092–1097.
16. Afrashi F, Erakgün T, Köse S, Ardıç K, Menteş J. Blue-on-yellow perimetry versus achromatic perimetry in type 1 diabetes patients without retinopathy. *Diabetes Res Clin Pract*. 2003;61:7–11.
17. Nitta K, Saito Y, Kobayashi A, Sugiyama K. Influence of clinical factors on blue-on-yellow perimetry for diabetic patients without retinopathy: comparison with white-on-white perimetry. *Retina*. 2006;26:797–802.
18. Zhou HP, Asaoka R, Inoue T, et al. Short wavelength automated perimetry and standard automated perimetry in central serous chorioretinopathy. *Sci Rep*. 2020;10:16451–16451.
19. Asahina Y, Kitano M, Hashimoto Y, et al. The structure-function relationship measured with optical coherence tomography and a microperimeter with auto-tracking: the MP-3, in patients with retinitis pigmentosa. *Sci Rep*. 2017;7:15766
20. Greenstein VC, Schuman AD, Lee W, et al. Near-infrared autofluorescence: its relationship to short-wavelength autofluorescence and optical coherence tomography in recessive Stargardt disease. *Invest Ophthalmol Vis Sci*. 2015;56:3226–3234.
21. Duncker T, Marsiglia M, Lee W, et al. Correlations among near-infrared and short-wavelength autofluorescence and spectral-domain optical coherence tomography in recessive Stargardt disease. *Invest Ophthalmol Vis Sci*. 2014;55:8134–8143.
22. Han L, de Carvalho JRL, Jr, Parmann R, et al. Central serous chorioretinopathy analyzed by multimodal imaging. *Transl Vis Sci Technol*. 2021;10:15.
23. Ayata A, Tatlipinar S, Kar T, Unal M, Ersanli D, Bilge AH. Near-infrared and short-wavelength autofluorescence imaging in central serous chorioretinopathy. *Br J Ophthalmol*. 2009;93:79–82.
24. Özmert E, Batioğlu F. Fundus autofluorescence before and after photodynamic therapy for chronic central serous chorioretinopathy. *Ophthalmologica*. 2009;223:263–268.

Investigative Ophthalmology & Visual Science